J. Plasma Phys. (2017), *vol.* 83, 655830101
doi:10.1017/S0022377816001276

Effective factors on twisted terahertz radiation generation in a rippled plasma

Hassan Sobhani[1],†, **Elham Dadar**[2] **and Sahar Feili**[3]

[1]Young Researchers and Elite Club, Qom Branch, Islamic Azad University, Qom, Iran

[2]Faculty of Economics, Mofid University of Qom, Qom, Iran

[3]Department of Physics, Shahid Bahonar University, Kerman, Iran

(Received 25 October 2016; revised 16 December 2016; accepted 20 December 2016)

Based on the beating of two Laguerre–Gaussian laser beams in a rippled plasma medium, the effective factors such as plasma density, Gouy phase and orbital angular momentums of input lasers on the output twisted terahertz radiation are investigated. As a result, the amplitude of the generated vortex terahertz radiation is an increasing function of plasma density. The vortex terahertz intensity is strongly dependent on the orbital angular momentum of the input lasers. The terahertz output amplitude increases by decreasing the orbital angular momentum of the Laguerre–Gaussian input lasers. Here, by employing a suitably ripple wavenumber, the destroyer effect of the relative Gouy phase of the input lasers is removed, and perfect phase matching is satisfied.

Key words: plasma applications, plasma nonlinear phenomena, plasma waves

1. Introduction

Optical vortex beams have attracted a great deal of attention related to research and for technological applications such as terabit high-speed communications, optical manipulation, optical vortex knots and chiral nanofabrication (Paterson *et al.* 2001; Grier 2003; Dennis *et al.* 2010; Omatsu *et al.* 2010; Toyoda *et al.* 2012; Wang *et al.* 2012; Bozinovic *et al.* 2013; Watabe *et al.* 2014). Vortex beams have an annular intensity profile, a spiral wave front and quantization orbital angular momentums (OAM) characterized by charge number l. Terahertz (THz) radiation sources (Malik 2015; Singh & Malik 2015, 2016) have been receiving increasing levels of interest in diverse areas such as biological imaging and sensing, surface chemistry and communications (Orenstein & Millis 2000; Lee 2009). The role of an external direct current (DC) magnetic field and femtosecond laser pulses in tuning the frequency and power of THz radiation have been surveyed (Malik, Malik & Kawata 2010; Malik & Malik 2012, 2013; Malik, Malik & Stroth 2012). Recently, different profile of lasers, such as super-Gaussian beams for obtaining more collimated THz radiation, have been investigated (Malik, Malik & Stroth 2011*b*; Malik & Malik 2012; Singh & Malik 2014).

† Email address for correspondence: Hassan960sob@gmail.com

THz vortices have great potential for many application such as manipulation of the rotations of a quantum condensate (because their elementary rotational excitations are found in the THz frequency range) (Sanvitto *et al.* 2010), optical manipulation of electron beams (Hebling *et al.* 2011), wireless communications (because they can support an infinite number of OAM eigenstates characterized by their topological charges) (Fickler *et al.* 2012), imaging and sensing in the medical fields (Pickwell & Wallace 2006), optical tweezers and biomedical engineering (Simpson *et al.* 1998; Humphreys *et al.* 2004). The conventional method for generating a vortex beam in optical frequency domain such as fork-shaped holograms (Heckenberg *et al.* 1992) and cylindrical lens converters (Beijersbergen *et al.* 2003) cannot be directly implemented in the THz frequency domain. A few works about the generation of THz vortices have been reported. Recently, a V-shaped antenna meta-surface structure to achieve phase modulation for cross-polarized scattered fields has been investigated (Yu *et al.* 2011). The design to build a vortex phase plate and generate an optical vortex in the infrared wave band has been utilized (Genevet *et al.* 2012). The complementary V-shaped antenna structure to generate a THz vortex beam, which requires precise control of the geometric parameters and azimuth of the V-shaped antenna structure, has been used (He *et al.* 2013). Other ways for generating twisted terahertz radiation, based on the angular momentum exchange between plasma vortex and the laser beam, have been proposed (Sobhani, Rooholamininejad & Bahrampour 2016*a*).

Twisted THz radiation generated by beating Laguerre–Gaussian (LG) lasers has been proposed in which the evolution of the beams width in plasma is considered (Sobhani, Rooholamininejad & Bahrampour 2016*b*). In this research, the effective factors such as plasma density, Gouy phase and orbital angular momentums of the input lasers on the output twisted terahertz radiation are investigated. Here the evolution of the beams width in plasma is ignored. The intensity variation in the transverse direction leads to a transverse nonlinear ponderomotive force that gives rise to a component of current oscillating at the beat frequency of the lasers. This plasma current has superluminal Fourier components, which can emit a THz wave. It is shown that this emitted vortex THz radiation generally is a superposition of two OAM. Here a suitable plasma density distribution is considered to produce THz radiation having only one OAM. Furthermore, by proposing the perfect phase matching condition, the destroyer effects of the relative Gouy phase of the laser beams is controlled.

The organization of this paper is as follows. In the second section, the theoretical model for the evaluation of nonlinear current density and emitted THz radiation amplitude is presented. The third section is dedicated to investigation of the effective parameters on emitted THz radiation amplitude. In the last section, the results are summarized.

2. Theoretical analysis

Consider the propagation of two coaxial high power vortex laser beams along the z-direction in the nonlinear plasma medium. It is supposed that the lasers electric field is polarized along the x-axis, with frequencies ω_1, ω_2 and wavenumbers k_1, k_2. The laser beams with LG distribution can be described by the phase singularity on axis with strength l that is called the optical vortex charge number, and by the radial index p. Here, the beam width evolution is ignored and the distribution of the laser beams is considered doughnut shaped ($p = 0$) as:

$$E_j = a_{0,l_j}(z) D_0^{l_j}(r, z) \mathrm{e}^{\mathrm{i}l_j\phi} \mathrm{e}^{\mathrm{i}k_j z - i\omega_j t}. \tag{2.1}$$

https://doi.org/10.1017/S0022377816001276 Published online by Cambridge University Press

While

$$D_0^{l_j}(r,z) = \left(\frac{\sqrt{2}r}{w_j}\right)^{|l_j|} \mathrm{e}^{-[1-i\beta(z)]r^2/w_j^2} \tag{2.2a}$$

$$a_{0,l_j}(z) = E_0 \left(\frac{2}{\pi(l_j)!}\right)^{1/2} \mathrm{e}^{\mathrm{i}\psi_{0,l_j}(z)}, \tag{2.2b}$$

where $j = 1, 2$. In (2.1), E_0 is the initial electric field amplitude, r_0 is the beam width, $\beta(z)$ is related to the curvature of wave front and $\psi_{0,l}(z)$ is the Gouy phase. The laser beams provide a nonlinear oscillatory velocity to the electrons due to the ponderomotive force, at the beat wave frequency $\tilde{\omega} = \omega_1 - \omega_2$ and wavenumber $\tilde{k} = k_1 - k_2$. This oscillation is perpendicular to the propagation direction of the lasers. Further, a space-periodically modulated plasma, $n = n_0 + n'$ is considered, where n_0 is background electron density. Also $n' = n_q \mathrm{e}^{\mathrm{i}qz}$, where n_q and q are the amplitude and wavenumber of the density ripple, respectively. The density ripple can be created by various techniques (Hazra *et al.* 2004; Antonsen Jr, Palastro & Milchberg 2007; Kuo *et al.* 2007), which operate as a slow wave structure that guides the phase matching condition and induces resonant excitation for generating higher THz radiation. The laser fields impart oscillatory velocities $\boldsymbol{v}_j = e\boldsymbol{E}_j/\mathrm{i}m\omega_j$ to the electrons, and furthermore exert a ponderomotive force, $\boldsymbol{F}^{NL} = m/2\nabla \boldsymbol{v}_1 \cdot \boldsymbol{v}_2^*$, at the beat wave frequency $\tilde{\omega}$ and wavenumber $\tilde{k}$. Considering equal beam width, the x-component of the nonlinear ponderomotive force due to beating of two LG lasers is obtained as

$$\begin{aligned} \boldsymbol{F}_x^{NL} = {} & \frac{e^2E_0^2}{\pi m\omega_1\omega_2\sqrt{l_1!l_2!}} \left(\frac{\sqrt{2}r}{r_0}\right)^{l_1+l_2} \mathrm{e}^{-2(r^2/r_0^2)} \left\{\cos\phi \left[\frac{l_1+l_2}{r} - 4\frac{r^2}{r_0^2}\right] - \frac{\mathrm{i}\tilde{l}}{r}\sin\phi\right\} \\ & \times \mathrm{e}^{\mathrm{i}\tilde{l}\phi} \mathrm{e}^{-\mathrm{i}\tilde{l}\tan^{-1}(z/z_R)} \mathrm{e}^{\mathrm{i}\tilde{k}z - \mathrm{i}\tilde{\omega}t}, \end{aligned} \tag{2.3}$$

where $\tilde{l} = l_1 - l_2$ and z_R is the Rayleigh length. The ponderomotive force is a superposition of two OAM. This ponderomotive force gives rise to the nonlinear perturbation, n^{NL}, in the electron density, that produces a space charge field. This space charge field self-consistently induces another type of density perturbation, n^L. Using the equations of motion and continuity of electrons we obtain n^L. By employed Poisson's equation, the potential of the space charge field, with the combined effects of both the perturbation in electron density, $n^L + n^{NL}$, can be derived. The electrostatic potential, ϕ, as the main source of perturbation, is obtained (Malik, Malik & Nishida 2011*a*)

$$\nabla\phi = -\frac{4\pi n_0 e}{m\tilde{\omega}^2\left(1 - \dfrac{\omega_p^2}{\tilde{\omega}^2}\right)} \boldsymbol{F}^{NL}. \tag{2.4}$$

Using the equation of motion, by taking into account the contribution of the self-consistent field, $e\nabla\phi$, and the ponderomotive force, $\boldsymbol{F}^{NL}$, the response of the electrons turns out to be

$$\boldsymbol{v}^{NL} = \frac{\mathrm{i}\tilde{\omega}}{m(\tilde{\omega}^2 - \omega_p^2)} \boldsymbol{F}^{NL}. \tag{2.5}$$

The intensity variation in the transverse direction produces a large change in the ponderomotive force that gives rise to a component of current oscillating at the beat frequency of the lasers. In the presence of ripple plasma density, the nonlinear current

https://doi.org/10.1017/S0022377816001276 Published online by Cambridge University Press

density is obtained as

$$\boldsymbol{J}^{NL} = -\frac{\mathrm{i}en_q \mathrm{e}^{\mathrm{i}qz}\tilde{\omega}}{2m(\tilde{\omega}^2 - \omega_p^2)}\boldsymbol{F}^{NL}. \tag{2.6}$$

Here the density perturbation is assumed to be small enough so that $n^L \ll n_q$. As is clear from (2.6), the current density changes in accordance with the nonlinear ponderomotive force, $\boldsymbol{F}^{NL} \sim \mathrm{e}^{\mathrm{i}\tilde{k}z - i\tilde{\omega}t}$. Since $\boldsymbol{J}^{NL}$ is responsible for the generation of THz radiation, the THz field will vary as $\mathrm{e}^{\mathrm{i}\tilde{k}z - i\tilde{\omega}t}$. Using Maxwell's equations, the THz wave equation is obtained as follows

$$-\nabla^2 \boldsymbol{E}_T + \boldsymbol{\nabla}(\boldsymbol{\nabla}\cdot\boldsymbol{E}_T) - \frac{\tilde{\omega}^2 - \omega_p^2}{c^2}\boldsymbol{E}_T = \frac{4\pi\mathrm{i}\tilde{\omega}}{c^2}\boldsymbol{J}^{NL}. \tag{2.7}$$

Taking the x-component of (2.7), the emitted THz radiation, in response to the nonlinear current, is a superposition of two OAM. By employing a suitable plasma density distribution, one of the OAM is eliminated. So THz radiation having one OAM can be generated. Here, the plasma density distribution is considered as $\omega_p^2 = \omega_{p0}^2[1 + b(l_T) + r^2/a^2]$, where $\omega_{p0} = (4\pi e^2 n_0^0/m)^{1/2}$, $b(l_T) = -(c^2/\omega_{p0}^2)(4(|l_T| + 1)/w_0^2)$ and $a = w_0^2\omega_{p0}/2c$. This electron density distribution can be produced by different sources of energy (Kaur, Sharma & Salih 2009; Sobhani *et al.* 2016*c*,*d*). The x-component of (2.7) can be deduced as

$$\left[\frac{\partial^2}{\partial r^2} + \frac{1}{r}\frac{\partial}{\partial r} + \frac{1}{r^2}\frac{\partial}{\partial \phi} + \frac{\partial^2}{\partial z^2}\right]E_T + \frac{\tilde{\omega}^2}{c^2}\varepsilon E_T = -\frac{4\pi i\tilde{\omega}}{c^2}J_x^{NL}, \tag{2.8}$$

where $\varepsilon = 1 - \omega_p^2/\tilde{\omega}^2$ is the permittivity of the plasma medium at the THz frequency $\tilde{\omega}$. By choosing suitable plasma parameters a and b, the first three terms on the left-hand side of (2.8) vanish, so the beam width evolution of THz field can be ignored and the vortex charge number of the generated twisted THz radiation is predicted. Using the separation of variables method, a homogeneous solution of (2.8) in the absence of the nonlinear current density, is given as (Sobhani *et al.* 2016*b*)

$$E_T(r, \phi, z) = A^{l_T}\left(\frac{\sqrt{2}r}{w_0}\right)^{|l_T|}\mathrm{e}^{-r^2/w_0^2}\mathrm{e}^{\mathrm{i}k_T z}\mathrm{e}^{\mathrm{i}l_T\phi}, \tag{2.9}$$

where the amplitude of the wave, A^{l_T} is a constant. It is expected on physical grounds that, when the nonlinear source term is not too large, the solution to (2.8) will still be of the form of (2.9), except that A^{l_T} will be a slowly varying function of z. So the solution may be written as

$$E_T(r, \phi, z) = A^{l_T}(z)\left(\frac{\sqrt{2}r}{w_0}\right)^{|l_T|}\mathrm{e}^{-r^2/w_0^2}\mathrm{e}^{\mathrm{i}k_T z}\mathrm{e}^{\mathrm{i}l_T\phi}. \tag{2.10}$$

This solution has a doughnut LG form in which the beam width, w_0 is related to the parameters of plasma density. So the plasma density distribution plays the fundamental role in the distribution of the emitted THz radiation. Also the charge number of the emitted THz radiation is determined by the parameters of plasma density. The fast phase variations in E_T are taken as $\mathrm{e}^{\mathrm{i}k_T z - i\tilde{\omega}t}$, and the phase matching condition demands

https://doi.org/10.1017/S0022377816001276 Published online by Cambridge University Press

$k_T = k_1 - k_2 + q$. Substituting (2.10) into (2.8), one obtains

$$\left[2ik_T\frac{\partial}{\partial z} + \left(\frac{\tilde{\omega}^2}{c^2}\varepsilon - k_T^2\right)\right] A^{l_T}(z)\left(\frac{\sqrt{2}r}{w_0}\right)^{|l_T|} e^{-r^2/w_0^2} e^{ik_T z} e^{il_T\phi} = \frac{-4\pi i\tilde{\omega}}{c^2} J_x^{NL}. \quad (2.11)$$

The beam width evolution of the THz radiation, w_0, in the nonlinear plasma is ignored. Using the definition of $k_T^2 = (\tilde{\omega}^2/c^2)\varepsilon$, the second term on the left-hand side of (2.11) vanishes. Under the resonant excitation of the THz radiation, the wavenumber of the rippled plasma density is given as $q = \tilde{\omega}/c[(1 - \omega_p^2/\tilde{\omega}^2)^{1/2} - 1]$. The normalized period of the density ripple structure, qc/ω_p, plays an important role in the phase matching and generation of efficient vortex THz radiation. Equation (2.11) is multiplied by $e^{-il'\phi}D_{p'}^{l'*}(\xi)$, where $\xi = 2r^2/w_0^2$, and integrated over r and ϕ. Using the orthogonality relations of $D_p^l(\xi)$ and $e^{il\phi}$, the value of the THz radiation amplitude is zero, except for two indexes. Therefore one can obtain

$$\left|\frac{\partial A^{l_T}(z)}{\partial z}\right| = \frac{n_q}{n_0^0}\frac{\omega_{p0}^2\tilde{\omega}^2 eE_0^2}{\omega_1\omega_2}\frac{e^{-i\tilde{l}\tan^{-1}(z/z_R)}e^{i(\tilde{k}+q-k_T)z}}{8\pi k_T c^2 m_e\sqrt{l_1!\ l_2!}|l_T|!} \times [(G_1^{\tilde{l}+1} - \tilde{l}G_2^{\tilde{l}+1})\delta_{\tilde{l}+1,l_T} + [(G_1^{\tilde{l}-1} + \tilde{l}G_2^{\tilde{l}-1})\delta_{\tilde{l}-1,l_T}]]. \quad (2.12)$$

While

$$G_1^{\tilde{l}+1} = \int_0^\infty \frac{4r}{w_0^2[\tilde{\omega}^2 - \omega_p^2(r)]}\left(\frac{l_1+l_2}{r} - \frac{4r}{r_0^2}\right)\left(\frac{\sqrt{2}r}{r_0}\right)^{l_1+l_2}\left(\frac{\sqrt{2}r}{w_0}\right)^{|\tilde{l}+1|} e^{-r^2(2/r_0^2+1/w_0^2)}\,dr \quad (2.13a)$$

$$G_1^{\tilde{l}-1} = \int_0^\infty \frac{4r}{w_0^2[\tilde{\omega}^2 - \omega_p^2(r)]}\left(\frac{l_1+l_2}{r} - \frac{4r}{r_0^2}\right)\left(\frac{\sqrt{2}r}{r_0}\right)^{l_1+l_2}\left(\frac{\sqrt{2}r}{w_0}\right)^{|\tilde{l}-1|} e^{-r^2(2/r_0^2+1/w_0^2)}\,dr \quad (2.13b)$$

$$G_2^{\tilde{l}+1} = \int_0^\infty \frac{4\,dr}{w_0^2[\tilde{\omega}^2 - \omega_p^2(r)]}\left(\frac{\sqrt{2}r}{r_0}\right)^{l_1+l_2}\left(\frac{\sqrt{2}r}{w_0}\right)^{|\tilde{l}+1|} e^{-r^2(2/r_0^2+1/w_0^2)} \quad (2.13c)$$

$$G_2^{\tilde{l}-1} = \int_0^\infty \frac{4dr}{w_0^2[\tilde{\omega}^2 - \omega_p^2(r)]}\left(\frac{\sqrt{2}r}{r_0}\right)^{l_1+l_2}\left(\frac{\sqrt{2}r}{w_0}\right)^{|\tilde{l}-1|} e^{-r^2(2/r_0^2+1/w_0^2)}. \quad (2.13d)$$

The plasma parameters, w_0 and $b(l_T)$, determine the characteristics of the THz radiation such as the beam width and the topological charge. By beating the two LG lasers having relative topological charge, $\tilde{l}$, in a plasma medium characterized by parameter $b(l_T)$, the THz amplitude is non-zero when $l_T = \tilde{l} \pm 1$. Equation (2.12) illustrates that the suitable plasma distribution, $b(\tilde{l} \pm 1)$, is emphasized that vortex THz radiation with only one OAM can be produced. The amplitude of the THz radiation generated can be written as

$$|A^{\tilde{l}\pm1}| = \frac{n_q}{n_0^0}\frac{\omega_{p0}^2\tilde{\omega}^2}{\omega_1\omega_2}\frac{eE_0^2[G_1^{\tilde{l}\pm1} \mp \tilde{l}\ G_2^{\tilde{l}\pm1}]}{8\pi k_T c^2 m_e(|\tilde{l} \pm 1|)!\sqrt{l_1!\ l_2!}}\int_0^z e^{-i\tilde{l}\tan^{-1}(z'/z_R)}e^{i(\tilde{k}+q-k_T)z'}\,dz'. \quad (2.14)$$

The features of the THz field amplitude due to the beating of the two lasers are solved numerically. Due to the relative Gouy phase, defined as the difference of

https://doi.org/10.1017/S0022377816001276 Published online by Cambridge University Press

the Gouy phases of the input lasers, the relative phase between the lasers plays an important role in the generation of the THz radiation. The relative Gouy phase induces a decrease in the amplitude of the THz radiation generation, as it is obvious from (2.14). If the topological numbers of the lasers are equal, $\tilde{l} = 0$, the Gouy phase shift of each laser is removed others and the amplitude of the THz radiation generation is higher.

3. Results and discussion

Recently, the generation of THz radiation by the beating of laser beams has attracted a great deal of attention related to research and technological applications. The interest in vortex waves in the THz domain can also be applied to data transmission (Wang *et al.* 2012), communications (Zhu *et al.* 2014) and active THz holography (Xie, Wang & Zhang 2013). Also, the THz frequency region includes the eigenfrequencies of molecules so THz imaging has been applied to biomedicine, security, and spectroscopy (Markelz, Roitberg & Heilweil 2000; Ferguson & Zhang 2002; Kawase *et al.* 2003; Chen *et al.* 2008; Zhang *et al.* 2009; Ohno *et al.* 2009, 2010). Here (2.14) is solved to study the features of the THz field amplitude for the following laser and plasma parameters; the frequencies of the laser beams are 2.4×10^{14} rad s^{-1} and 2.1×10^{14} rad s^{-1}, also the initial beam width of both lasers is 50 μm and the plasma frequency is 2.75×10^{14} rad s^{-1}. The plasma frequency should be selected to be lower than $\tilde{\omega}$ so that the THz wave can propagate in the plasma medium. The value of the normalized ripple amplitude is $n_q/n_0^0 = 0.1$ and the parameter of plasma density, related to the THz radiation beam width, w_0, is 75 μm. When an intense laser encounters plasma, a ponderomotive force pushes the electrons out of strong power region, decreasing the local electron density, which leads to the further growth of the plasma dielectric function and consequently, an even stronger self-focusing of laser take places. The diffraction causes defocusing of the laser beams. Under the competition between the ponderomotive force effect and beam diffraction, periodic self-focusing and defocusing occurs and a density-modulated filament is created. Therefore intensity variation of LG lasers in the transverse direction is strong, and the plasma current or laser ponderomotive force can generate a THz wave at the beating frequency (Sobhani *et al.* 2016*b*).

For studying the effect of the topological charge of the incident lasers, the variation of the normalized THz field amplitude versus normalized propagation distance, $Z = z/z_R$, for different values of topological charge of input lasers is presented in figure 1. As seen, the normalized field amplitude of the emitted THz radiation for different OAM is non-similar, through the plasma density characterized by parameter $b(\tilde{l} \pm 1)$. One of these plasma parameters is such that the electron density is higher and the number of charge carriers involved in the generation of the oscillatory current is greater. Higher oscillatory current results in a higher vortex THz radiation. Because the pumps depletion effect is ignored, the THz amplitude is a rising function of z, and in the presence of the pump depletion effect it is expected that the output THz amplitude approaches a saturation value. The presence of the pump depletion effect is under study by our group and results will appear in the near future. Also, it is obvious from figure 1 that the THz field amplitude generated is higher when a lower vortex charge number is chosen. With the lower vortex charge number, the beam focusing–defocusing oscillations occur strongly; the density-modulated filament induces hardly any intensity variation in the transverse direction, and the ponderomotive force can generate higher THz radiation at the beat frequency. This fact is clear from (2.14).

https://doi.org/10.1017/S0022377816001276 Published online by Cambridge University Press

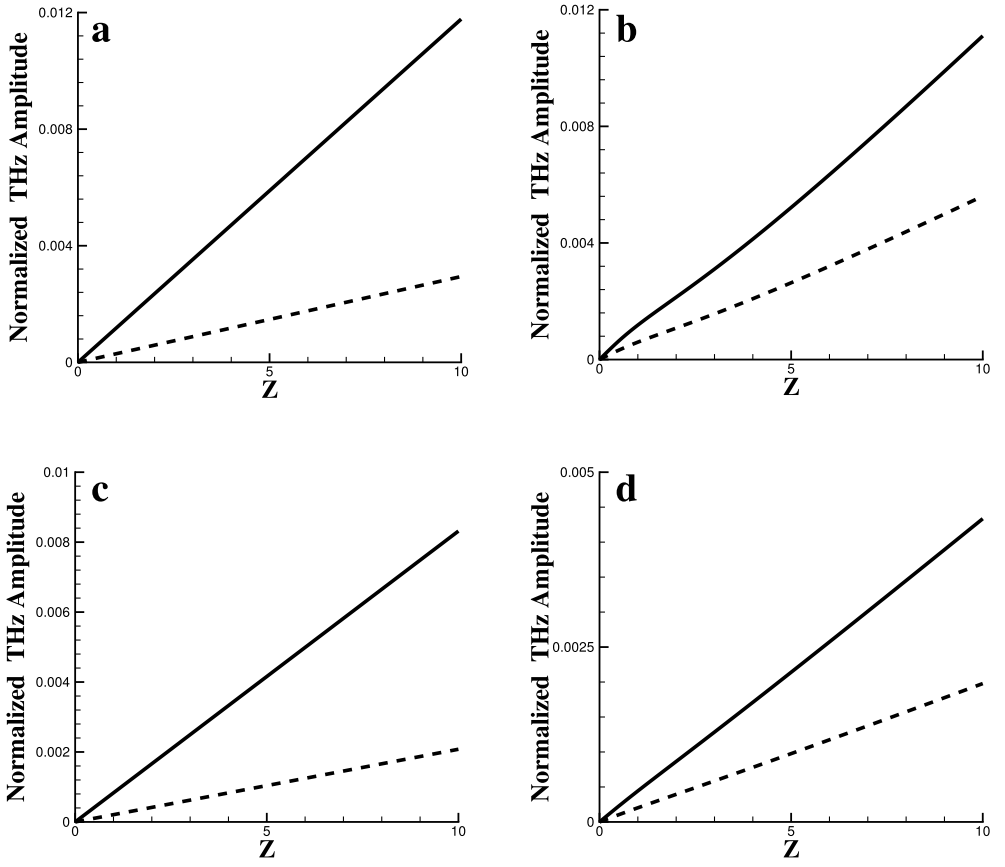

FIGURE 1. Normalized THz amplitude versus normalized propagation distance. The cases shown are, (*a*) $l_1 = 1$, $l_2 = 1$, for $l_T = 1$ (solid line), $l_T = -1$ (dashed line), (*b*) $l_1 = 2$, $l_2 = 0$, for $l_T = 3$ (solid line), $l_T = 1$ (dashed line), (*c*) $l_1 = 2$, $l_2 = 0$, for $l_T = 3$ (solid line), $l_T = 1$ (dashed line) and (*d*) $l_1 = 3$, $l_2 = 2$, for $l_T = 2$ (solid line), $l_T = 0$ (dashed line), in *b* (l_T) plasma distribution.

For instance, by beating two vortex lasers having charge numbers $l_1 = 2$ and $l_2 = 1$, THz radiation with OAM of $l_T = 2, 0$ is generated. The variation of the normalized THz field amplitude versus normalized propagation distance for different values of the normalized ripple amplitude is presented in figure 2. As seen in this figure, the THz field amplitude generated is higher when a larger value of the normalized ripple amplitude is selected. For clarification, a larger value of the normalized ripple amplitude is acquired for better phase matching and maximum energy transfer to the THz radiation. The growth in the THz field amplitude with the ripple amplitude is appreciable as larger numbers of electrons take part (in phase) in the oscillating nonlinear current. In figure 3, the intensity profiles of the input lasers (having charge numbers 2 and 1) and generated vortex THz, having charge numbers 2 and 0, are depicted.

The evolution of the normalized THz field amplitude as a function of the normalized propagation distance for different background plasma frequencies, ω_0^0, is shown in figure 4. Similar to the effect of ripple amplitude, the enhanced field with the growth in background plasma frequency is plausible as more electrons take part in

https://doi.org/10.1017/S0022377816001276 Published online by Cambridge University Press

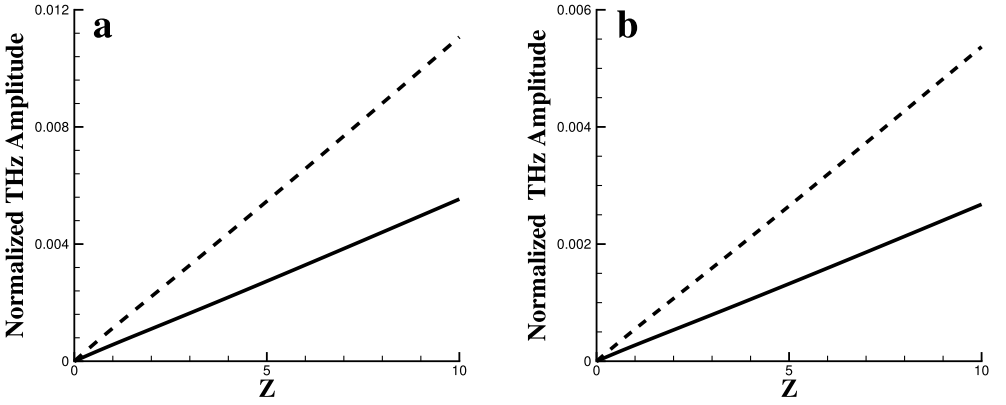

FIGURE 2. Normalized THz amplitude versus normalized propagation distance by beating of lasers having $l_1 = 2$, $l_2 = 1$, when the normalized ripple amplitude of $n_q = 0.1n_0$ (solid line) and $n_q = 0.2n_0$ (dashed line), for (*a*) $l_T = 2$, (*b*) $l_T = 0$ in corresponded plasma distribution.

the oscillating nonlinear current. For generating strong THz radiation, the plasma frequency should be near to the value of the beat wave frequency, $\omega_p \approx \omega$, this corresponds to the resonance condition so maximum energy transfer will occur.

Another parameter for generating strong THz radiation is the wavenumber of the density ripple. The expression in (2.14) predicts a dramatic decrease in the efficiency of the THz radiation generation process when the relative Gouy phase of the incident lasers is non-zero. By using the ripple wavenumber, considered in the previous section, perfect phase matching is not provided. Consequently, the THz radiation generated will be weak. By considering a new ripple wavenumber, $q = \tilde{\omega}/c[(1 - \omega_p^2/\tilde{\omega}^2)^{1/2} - 1] + \tilde{l}/z \tan^{-1}(z/z_R)$, which can be created by various techniques (Kaur *et al.* 2009; Sobhani *et al.* 2016*c*,*d*), one may define the perfect phase matching condition as $k_T = k_1 - k_2 - (\tilde{l}/z) \tan^{-1}(z/z_R) + q$. In the presence of this ripple wavenumber, the effect of the relative Gouy phases of the input lasers is removed and perfect phase matching is achieved. With this condition, the interaction length is infinite and the energy transfer from the pump laser to the emitted THz radiation will be maximized. A comparison of the generation of the THz radiation between the two phase matching conditions is presented in figure 5. This new ripple wavenumber is constructed at smaller distances and maximum energy transfer will happen. So efficient THz radiation generation will result.

In order to uncover the role of the beam width value of the incident lasers, the variation of the normalized THz field amplitude versus normalized propagation distance is illustrated in figure 6. As shown, the THz field amplitude decreases for the greater beam width. This observation is clear with regards to the beam width in the distribution of the LG beam. The ratio of the beam width of the input lasers r_0 to the parameter of plasma density, related to the beam width of the THz radiation w_0, is found to play an important role to the mechanism of generation of the THz radiation. Figure 7 gives the variation of the normalized THz amplitude as a function of the normalized propagation for different r_0/w_0. For $w_0 = 1.4r_0$, the slope of plasma density is greater than that for $w_0 = 1.5r_0$; so the transverse variation and ponderomotive force of the input lasers for the first case is greater and the THz radiation efficiency is better.

https://doi.org/10.1017/S0022377816001276 Published online by Cambridge University Press

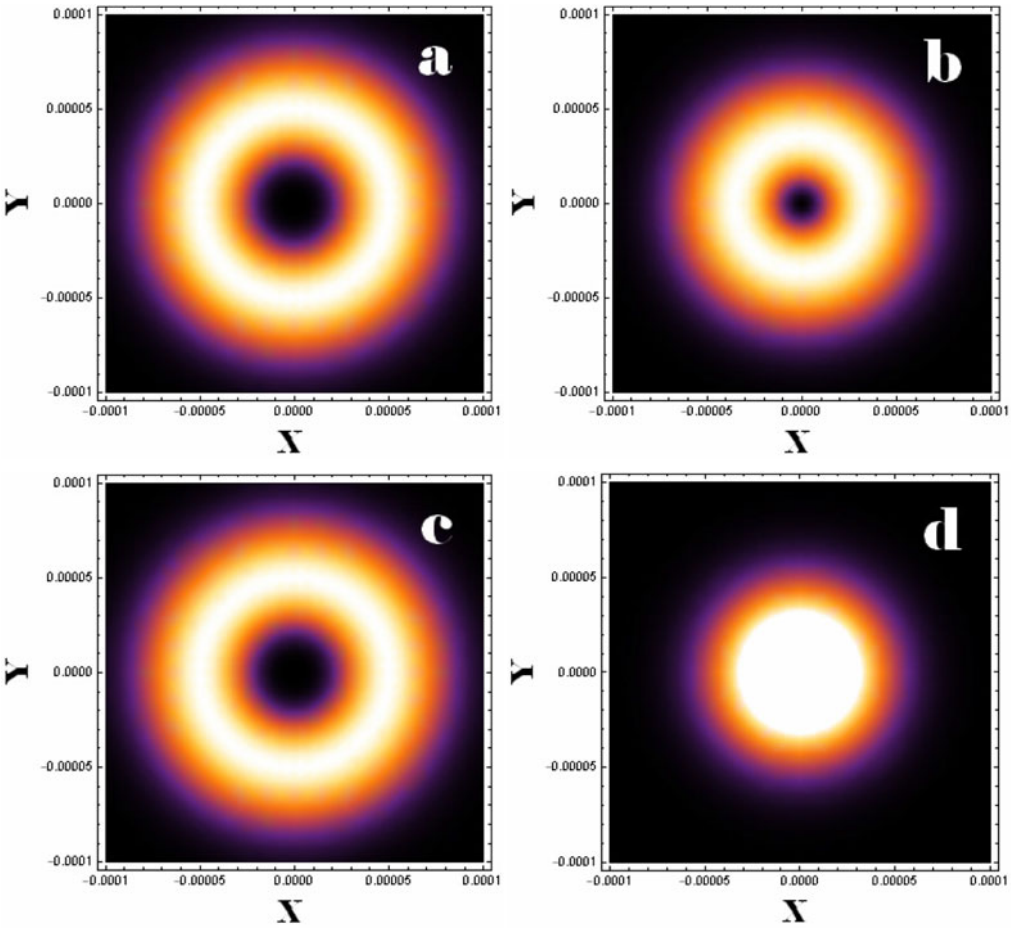

FIGURE 3. Profile of the input lasers and generated THz radiation: the topological charge numbers of the lasers are $l_1 = 2$ (*a*) and $l_2 = 1$ (*b*), and the topological charge numbers of the generated THz radiation are $l_T = 2$ (*c*) and (*d*) $l_T = 0$, in corresponded plasma distribution.

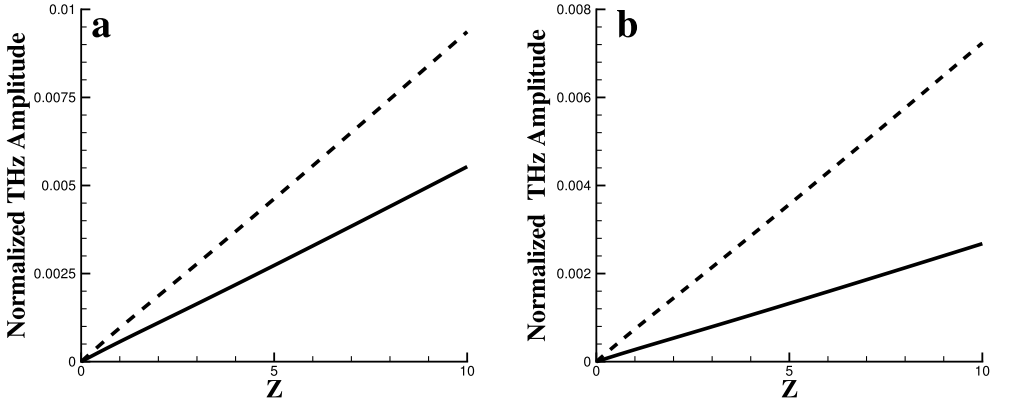

FIGURE 4. Normalized THz amplitude versus normalized propagation distance by beating of lasers having $l_1 = 2$, $l_2 = 1$, when $\omega_p = 2.7 \times 10^{13}$ rad s^{-1} (solid line) and $\omega_p = 2.5 \times 10^{13}$ rad s^{-1} (dashed line) for (*a*) $l_T = 2$, (*b*) $l_T = 0$ in corresponded plasma distribution.

https://doi.org/10.1017/S0022377816001276 Published online by Cambridge University Press

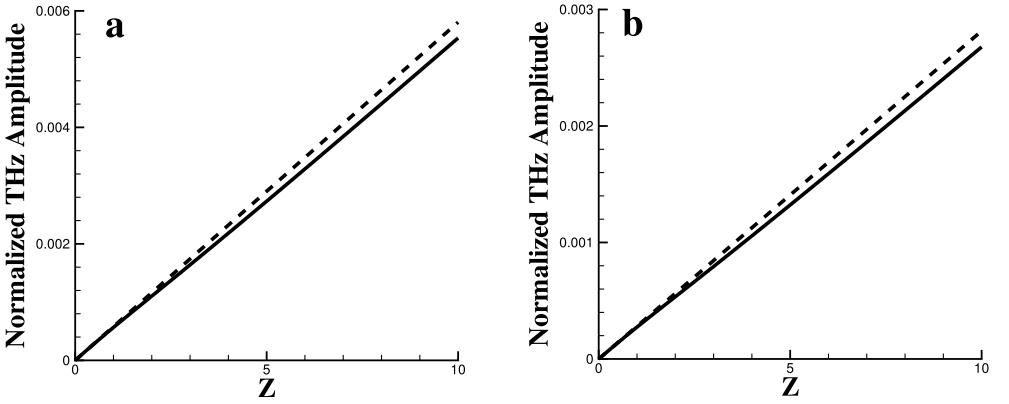

FIGURE 5. Normalized THz amplitude versus normalized distance by beating of lasers having $l_1 = 2$, $l_2 = 1$, under the phase matching condition, $k_T = k_1 - k_2 + q$ (solid line) and $k_T = k_1 - k_2 - \tilde{l}/z \tan^{-1}(z/z_R) + q$ (dashed line) for (*a*) $l_T = 2$, and (*b*) $l_T = 0$ in corresponded plasma density.

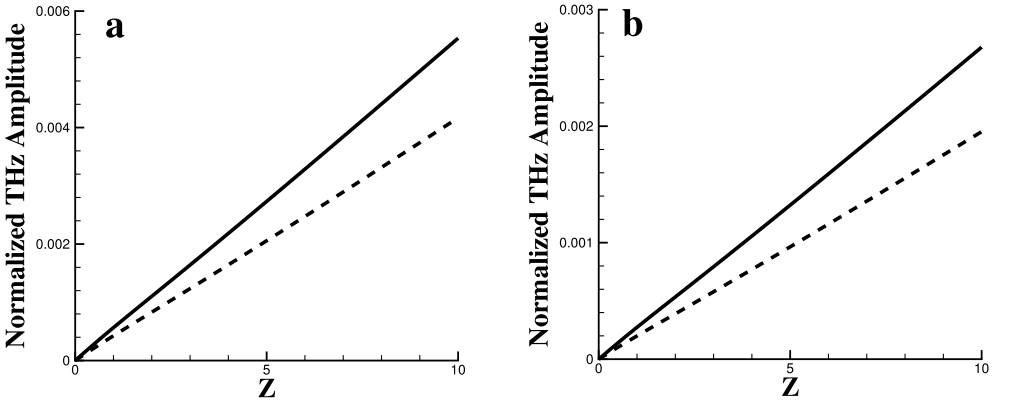

FIGURE 6. Normalized THz amplitude versus normalized propagation distance by beating of lasers having $l_1 = 2$, $l_2 = 1$ and $r_0 = 50$ μm (solid line), $r_0 = 40$ μm (dashed line) for (*a*) $l_T = 2$ and (*b*) $l_T = 0$ in corresponded plasma distribution.

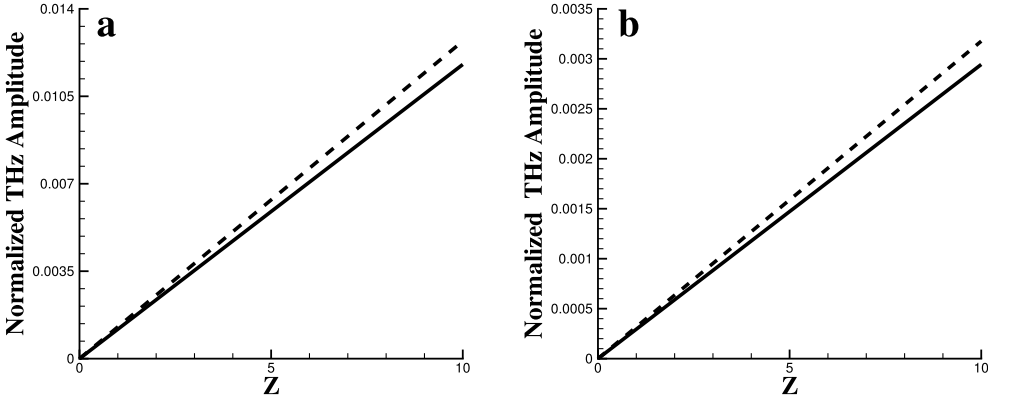

FIGURE 7. Normalized THz amplitude generated by beating of the lasers having $l_1 = 1$, $l_2 = 1$, versus normalized propagation distance for THz radiation beam width $w_0 = 1.5r_0$ (solid line) and $w_0 = 1.4r_0$ (dashed line), *viz.*, (*a*) $l_T = 2$, (*b*) $l_T = 0$ in corresponded plasma distribution.

https://doi.org/10.1017/S0022377816001276 Published online by Cambridge University Press

4. Conclusion

In conclusion, the present study surveys the effective parameters for the generation of vortex THz radiation. This work establishes that by beating of two LG lasers in a rippled plasma medium, a THz vortex having one OAM can be generated. Based on this method, a THz vortex with a higher charge number can be generated. The OAM of the vortex THz radiation opens avenues for new technologies in sensing, manipulation and telecommunication in the THz domain. For example, the annular THz vortex can be focused beyond the diffraction limit, so the THz vortex will potentially be used for super-resolution imaging and nonlinear spectroscopy in the biological sciences, non-destructive evaluation and security applications.

REFERENCES

ANTONSEN, T. M. JR, PALASTRO, J. & MILCHBERG, H. M. 2007 Excitation of terahertz radiation by laser pulses in nonuniform plasma channels. *Phys. Plasmas* **14** (3), 033107.

BEIJERSBERGEN, M., ALLEN, L., VAN DER VEEN, H. E. L. O. & WOERDMAN, J. 2003 Astigmatic laser mode converters and transfer of orbital angular momentum. *Optical Angular Momentum* **96**, 123.

BOZINOVIC, N., YUE, Y., REN, Y., TUR, M., KRISTENSEN, P., HUANG, H., WILLNER, A. E. & RAMACHANDRAN, S. 2013 Terabit-scale orbital angular momentum mode division multiplexing in fibers. *Science* **340** (6140), 1545–1548.

CHEN, H.-T., O'HARA, J. F., AZAD, A. K., TAYLOR, A. J., AVERITT, R. D., SHREKENHAMER, D. B. & PADILLA, W. J. 2008 Experimental demonstration of frequency-agile terahertz metamaterials. *Nat. Photon.* **2** (5), 295–298.

DENNIS, M. R., KING, R. P., JACK, B., OHOLLERAN, K. & PADGETT, M. J. 2010 Isolated optical vortex knots. *Nat. Phys.* **6** (2), 118–121.

FERGUSON, B. & ZHANG, X.-C. 2002 Materials for terahertz science and technology. *Nat. Mater.* **1** (1), 26–33.

FICKLER, R., LAPKIEWICZ, R., PLICK, W. N., KRENN, M., SCHAEFF, C., RAMELOW, S. & ZEILINGER, A. 2012 Quantum entanglement of high angular momenta. *Science* **338** (6107), 640–643.

GENEVET, P., YU, N., AIETA, F., LIN, J., KATS, M. A., BLANCHARD, R., SCULLY, M. O., GABURRO, Z. & CAPASSO, F. 2012 Ultra-thin plasmonic optical vortex plate based on phase discontinuities. *Appl. Phys. Lett.* **100** (1), 013101.

GRIER, D. G. 2003 A revolution in optical manipulation. *Nature* **424** (6950), 810–816.

HAZRA, S., CHINI, T. K., SANYAL, M. K., GRENZER, J. & PIETSCH, U. 2004 Ripple structure of crystalline layers in ion-beam-induced si wafers. *Phys. Rev.* B **70** (12), 121307.

HE, J., WANG, X., HU, D., YE, J., FENG, S., KAN, Q. & ZHANG, Y. 2013 Generation and evolution of the terahertz vortex beam. *Opt. Express* **21** (17), 20230–20239.

HEBLING, J., FÜLÖP, J. A., MECHLER, M. I., PÁLFALVI, L., TŐKE, C. & ALMÁSI, G. 2011 Optical manipulation of relativistic electron beams using thz pulses. arXiv:1109.6852.

HECKENBERG, N. R., MCDUFF, R., SMITH, C. P., RUBINSZTEIN-DUNLOP, H. & WEGENER, M. J. 1992 Laser beams with phase singularities. *Opt. Quant. Electron.* **24** (9), S951–S962.

HUMPHREYS, K., LOUGHRAN, J. P., GRADZIEL, M., LANIGAN, W., WARD, T., MURPHY, J. A. & O'SULLIVAN, C. 2004 Medical applications of terahertz imaging: a review of current technology and potential applications in biomedical engineering. In *Engineering in Medicine and Biology Society, 2004. IEMBS'04. 26th Annual International Conference of the IEEE*, vol. 1, pp. 1302–1305.

KAUR, S., SHARMA, A. K. & SALIH, H. A. 2009 Resonant second harmonic generation of a Gaussian electromagnetic beam in a collisional magnetoplasma. *Phys. Plasmas* **16** (4), 042509.

KAWASE, K., OGAWA, Y., WATANABE, Y. & INOUE, H. 2003 Non-destructive terahertz imaging of illicit drugs using spectral fingerprints. *Opt. Express* **11** (20), 2549–2554.

KUO, C.-C., PAI, C.-H., LIN, M.-W., LEE, K.-H., LIN, J.-Y., WANG, J. & CHEN, S.-Y. 2007 Enhancement of relativistic harmonic generation by an optically preformed periodic plasma waveguide. *Phys. Rev. Lett.* **98** (3), 033901.

LEE, Y.-S. 2009 *Principles of Terahertz Science and Technology,* vol. 170. Springer Science and Business Media.

MALIK, A. K. & MALIK, H. K. 2013 Tuning and focusing of terahertz radiation by DC magnetic field in a laser beating process. *IEEE J. Quant. Electron.* **49** (2), 232–237.

MALIK, A. K., MALIK, H. K. & KAWATA, S. 2010 Investigations on terahertz radiation generated by two superposed femtosecond laser pulses. *J. Appl. Phys.* **107** (11), 113105.

MALIK, A. K., MALIK, H. K. & NISHIDA, Y. 2011*a* Terahertz radiation generation by beating of two spatial-gaussian lasers. *Phys. Lett.* A **375** (8), 1191–1194.

MALIK, A. K., MALIK, H. K. & STROTH, U. 2011*b* Strong terahertz radiation by beating of spatial-triangular lasers in a plasma. *Appl. Phys. Lett.* **99** (7), 071107.

MALIK, A. K., MALIK, H. K. & STROTH, U. 2012 Terahertz radiation generation by beating of two spatial-Gaussian lasers in the presence of a static magnetic field. *Phys. Rev.* E **85** (1), 016401.

MALIK, H. K. 2015 Terahertz radiation generation by lasers with remarkable efficiency in electron–positron plasma. *Phys. Lett.* A **379** (43), 2826–2829.

MALIK, H. K. & MALIK, A. K. 2012 Strong and collimated terahertz radiation by super-Gaussian lasers. *Europhys. Lett.* **100** (4), 45001.

MARKELZ, A. G., ROITBERG, A. & HEILWEIL, E. J. 2000 Pulsed terahertz spectroscopy of DNA, bovine serum albumin and collagen between 0.1 and 2.0 THz. *Chem. Phys. Lett.* **320** (1), 42–48.

OHNO, S., HAMANO, A., MIYAMOTO, K., SUZUKI, C. & ITO, H. 2009 Surface mapping of carrier density in a gan wafer using a frequency-agile thz source. *J. Eur. Opt. Soc.-Rapid Publications* **4**.

OHNO, S., MIYAMOTO, K., MINAMIDE, H. & ITO, H. 2010 New method to determine the refractive index and the absorption coefficient of organic nonlinear crystals in the ultra-wideband thz region. *Opt. Express* **18** (16), 17306–17312.

OMATSU, T., CHUJO, K., MIYAMOTO, K., OKIDA, M., NAKAMURA, K., AOKI, N. & MORITA, R. 2010 Metal microneedle fabrication using twisted light with spin. *Opt. Express* **18** (17), 17967–17973.

ORENSTEIN, J. & MILLIS, A. J. 2000 Advances in the physics of high-temperature superconductivity. *Science* **288** (5465), 468–474.

PATERSON, L., MACDONALD, M. P., ARLT, J., SIBBETT, W., BRYANT, P. E. & DHOLAKIA, K. 2001 Controlled rotation of optically trapped microscopic particles. *Science* **292** (5518), 912–914.

PICKWELL, E. & WALLACE, V. P. 2006 Biomedical applications of terahertz technology. *J. Phys.* D*: Appl. Phys.* **39** (17), R301.

SANVITTO, D., MARCHETTI, F. M., SZYMAŃSKA, M. H., TOSI, G., BAUDISCH, M., LAUSSY, F. P., KRIZHANOVSKII, D. N., SKOLNICK, M. S., MARRUCCI, L., LEMAITRE, A. *et al.* 2010 Persistent currents and quantized vortices in a polariton superfluid. *Nat. Phys.* **6** (7), 527–533.

SIMPSON, N. B., MCGLOIN, D., DHOLAKIA, K., ALLEN, L. & PADGETT, M. J. 1998 Optical tweezers with increased axial trapping efficiency. *J. Mod. Opt.* **45** (9), 1943–1949.

SINGH, D. & MALIK, H. K. 2014 Terahertz generation by mixing of two super-Gaussian laser beams in collisional plasma. *Phys. Plasmas* **21** (8), 083105.

SINGH, D. & MALIK, H. K. 2015 Enhancement of terahertz emission in magnetized collisional plasma. *Plasma Sources Sci. Technol.* **24** (4), 045001.

SINGH, D. & MALIK, H. K 2016 Emission of strong terahertz pulses from laser wakefields in weakly coupled plasma. *Nucl. Instrum. Meth. Phys. Res.* A **829**, 403.

SOBHANI, H., ROOHOLAMININEJAD, H. & BAHRAMPOUR, A. R. 2016*a* Creation of twisted terahertz waves carrying orbital angular momentum via a plasma vortex. *J. Phys.* D*: Appl. Phys.* **49**, 295107.

SOBHANI, H., ROOHOLAMININEJAD, H. & BAHRAMPOUR, A. R. 2016*b* Terahertz twisted beams generation in plasma. *Eur. Phys. J.* D **70**, 168.

SOBHANI, H., VAZIRI, M., ROOHOLAMININEJAD, H. & BAHRAMPOUR, A. R. 2016*c* Impact of nonlinear absorption on propagation of microwave in a plasma filled rectangular waveguide. *Waves in Random Complex Media* **26**, 272.

SOBHANI, H., VAZIRI, M., ROOHOLAMININEJAD, H. & BAHRAMPOUR, A. R. 2016*d* Nonlinear interaction of intense hypergeometric Gaussian subfamily laser beams in plasma. *Opt. Laser Technol.* **81**, 40.

TOYODA, K., MIYAMOTO, K., AOKI, N., MORITA, R. & OMATSU, T. 2012 Using optical vortex to control the chirality of twisted metal nanostructures. *Nano Lett.* **12** (7), 3645–3649.

WANG, J., YANG, J.-Y., FAZAL, I. M., AHMED, N., YAN, Y., HUANG, H., REN, Y., YUE, Y., DOLINAR, S., TUR, M. *et al.* 2012 Terabit free-space data transmission employing orbital angular momentum multiplexing. *Nat. Photon.* **6** (7), 488–496.

WATABE, M., JUMAN, G., MIYAMOTO, K. & OMATSU, T. 2014 Light induced conch-shaped relief in an azo-polymer film. *Sci. Rep.* **4**.

XIE, Z., WANG, X. & ZHANG, Y. 2013 Active terahertz holography. In *International Conference on Optical Instruments and Technology (OIT2013)*, 90470B.

YU, N., GENEVET, P., KATS, M. A., AIETA, F., TETIENNE, J.-P., CAPASSO, F. & GABURRO, Z. 2011 Light propagation with phase discontinuities: generalized laws of reflection and refraction. *science* **334** (6054), 333–337.

ZHANG, S., PARK, Y.-S., LI, J., LU, X., ZHANG, W. & ZHANG, X. 2009 Negative refractive index in chiral metamaterials. *Phys. Rev. Lett.* **102** (2), 023901.

ZHU, L., WEI, X., WANG, J., ZHANG, Z., LI, Z., ZHANG, H., LI, S., WANG, K. & LIU, J. 2014 Experimental demonstration of basic functionalities for 0.1-thz orbital angular momentum (oam) communications. In *Optical Fiber Communication Conference*, p. M3K–7. Optical Society of America.

https://doi.org/10.1017/S0022377816001276 Published online by Cambridge University Press